PCCP

PAPER

View Article Online
View Journal | View Issue

Cite this: *Phys. Chem. Chem. Phys.*, 2015, **17**, 17182

Received 16th March 2015,
Accepted 27th May 2015

DOI: 10.1039/c5cp01525a

www.rsc.org/pccp

Giant magnetocrystalline anisotropy of 5d transition metal-based phthalocyanine sheet†

Jian Zhou,*[a] Qian Wang,[bca] Qiang Sun,[cba] Yoshiyuki Kawazoe[d] and Puru Jena*[a]

Large magnetocrystalline anisotropy energy (MAE) is a critical requirement for nanomagnets for applications in magnetic memory and storage devices. Due to small spin–orbit interaction the MAE of ferromagnetic films or single molecule magnets based on 3d metals is small and in typical magnetic nanostructures it is of the order of 2–3 meV. We show that MAE as high as 140 meV can be achieved by applying an external electric field or a biaxial tensile strain to phthalocyanine sheets decorated by 5d transition metal atoms such as Os and Ir. Our observation is based on a systematic study of 5d transition metal absorbed ploy phthalocyanine (Pc) sheets using first-principles density functional theory (DFT) combined with self consistently determined Hubbard *U* that accounts for the strong correlation energy. We attribute the high MAE values to d_{xy} and $d_{x^2-y^2}$ (d_{xz} and d_{yz}) interaction in Ir (Os) adsorbed structure.

I. Introduction

Magnetocrystalline anisotropy is associated with the directional dependence of a material's magnetic properties. Magnetocrystalline anisotropy energy (MAE) of a magnetically anisotropic material is defined as the energy difference between the low-energy magnetic moment aligned along the easy axis and the hard axis. For practical applications of magnetic materials in magnetic memory and storage devices, one necessary condition is to have large MAE so that the spin remains locked along its easy axis in spite of thermal fluctuations.[1,2] Typical TM-based nanostructures possess MAE less than 2–3 meV, which is very low and spins can be easily flipped under thermal fluctuations. Therefore, it is of considerable interest to fabricate materials with larger MAE.[3] Since magnetocrystalline anisotropy originates from the combined effect of the anisotropy in the atom's orbital magnetic moment (L) and its interaction with the atom's spin angular momentum (S), larger is this intra-atomic spin–orbit coupling (SOC) interaction, larger is the MAE. In most magnetic compounds L is either quenched or reduced, leading to small MAE values. One of the strategies to enhance MAE, therefore, has been to use low-coordination geometries. Recently, it was found that MAE as high as 58 meV can be achieved by depositing a Co atom above the O-site in a MgO monolayer grown on Ag(100).[3]

In this paper we use a different approach; we study a two-dimensional organometallic sheet (2D-OMS) decorated with transition metal atoms. We show that the MAE values can be enhanced as high as 140 meV by applying external electric field or biaxial tensile strain. The most important advantage of the 2D-OMS is that it contains well defined sites where transition metals (TM) can reside, thus providing stable and robust electronic, magnetic, and optical properties.[4–9] Note that in traditional dilute magnetic semiconductors (DMS) such as Mn doped GaN and GaAs, the TM atoms tend to cluster and the geometric structure is highly dependent on the synthesis process.[10,11] Similarly, embedding TM atoms in graphene and BN would require well defined and periodically arranged vacancies which are difficult to achieve experimentally.[12–14] In addition, vacancies can adversely affect the structure and chemical integrity of the substrate. Furthermore, compared to the self-assembled organometallic molecules on metal surfaces,[15,16] these 2D polymerized structures are stable and can be exfoliated.

Recently, Abel *et al.* have successfully fabricated a novel 2D-OMS polymer composed of Fe embedded phthalocyanine (Pc) sheet.[17] Due to the flexibility of the central site in Pc, other TM-based 2D polymers have also been realized experimentally. For example, polymeric Mn-based Pc (denoted as poly-MnPc) can also be formed upon annealing on-surface.[18] Thus, ploy-Pc sheets provide a new platform to study 2D-OMS by embedding different TM atoms. This series of poly-TMPc systems exhibit promising applications in magnetic memory, gas storage and capture, electronic circuits, quantum Hall effect, spintronics, and catalysis.[19–23]

Using first-principles calculations we have earlier shown that these poly-TMPc sheets are magnetic with robust coupling

[a] *Physics Department, Virginia Commonwealth University, Richmond, VA 23284, USA. E-mail: jzhou2@vcu.edu, pjena@vcu.edu*
[b] *Center for Applied Physics and Technology, College of Engineering, Peking University, Beijing 100871, China*
[c] *Department of Materials Science and Engineering, College of Engineering, Peking University, Beijing 100871, China*
[d] *Institute for Material Research, Tohoku University, Sendai, 980-8577, Japan*

† Electronic supplementary information (ESI) available. See DOI: 10.1039/c5cp01525a

between the TM atoms.[19] However, most of these are antiferromagnetically coupled, hindering their potential usage as magnetic memory devices. Only the poly-MnPc was found to exhibit ferromagnetic coupling, but the exchange coupling is weak – its Curie temperature was estimated to be ~150 K by Monte-Carlo simulations. Upon carrier doping, the antiferromagnetic systems (poly-CrPc and poly-FePc) can be tuned to be ferromagnetic, but their Curie temperatures are still lower than the room temperature.[23]

Our interest in this paper is to design poly-TMPc based nanostructures with large MAE. We note that magnetic anisotropy originates from intra-atomic spin–orbital coupling (SOC) interactions. Compared with 3d/4d TM atoms, heavier 5d elements usually exhibit large SOC. Besides, it has been reported that when a TM atom dimer is adsorbed on a substrate, the MAE is much larger than that of a single adsorbed TM atom.[24–31] In this paper we calculate the MAEs of a series of 5d TM atoms adsorbed poly-TMPc frameworks using first-principles density functional theory (DFT). The effect of strong correlation is taken into account within the context of Hubbard U calculated self-consistently within linear response theory. As the energy variation is marginal when the magnetic axis lies in the x–y plane, the MAE is defined as MAE = $E_{\parallel} - E_{\perp}$, where $E_{\parallel}$ and $E_{\perp}$ are energies of when the 5d TM atom magnetic axis is parallel or perpendicular to the Pc planar framework, respectively. In order to lock the magnetic axis pointing either along z or $-z$ direction, the MAE value should be positive and large. A typical structure with different orientation is shown in Fig. 1a and b. In this work we denote this framework as poly-(A,B)Pc, where A = Os, Ir, and B = Fe, Co, Ru, Rh, Os, Ir. Only Fe- and Co-group elements are considered because they can exhibit large magnetic moment and large MAE in their isolated dimer state.[19,24] In order to account for the strong electron correlation of the 5d magnetic TM accurately, we perform DFT + U calculations with the on-site Coulomb interaction U term determined self-consistently from first-principles.[32] Without any external perturbation we find the MAEs of most poly-(A,B)Pc systems to be negative, *i.e.*, the easy axis aligns in the x–y plane. Only in a few cases the MAEs are positive, but small.

In order to enhance the MAE values, we use two strategies – applying an external vertical electric field (E-field) or a biaxial tensile strain to the poly-(Ir,Ir)Pc, poly-(Ir,Rh)Pc, and poly-(Os,Os)Pc. The large MAE value originates from the interaction between the d_{xy} and $d_{x^2-y^2}$ of the absorbed Ir (atom A) in the poly-(Ir,Ir)Pc and poly-(Ir,Rh)Pc, and between the d_{xz} and d_{yz} of the absorbed Os (atom A) in the poly-(Os,Os)Pc.

II. Computational methods

Our calculations are based on density functional theory (DFT) and spin polarized generalized gradient approximation (GGA) prescribed by Perdew–Burke–Ernzerhof (PBE)[33] and implemented in Vienna Ab initio Simulation Package (VASP).[34] Periodic boundary condition and vacuum space of 15 Å along the z direction are used in order to avoid interactions between nearest neighbor image. Projector augmented wave (PAW) method[35,36] and plane wave basis set with a kinetic energy cutoff of 400 eV is used. The valence electrons of Fe- and Co-group TM atoms are 8 and 9, respectively. The Vosko–Wilk–Nusair modification scheme is applied to interpolate the correlation energy in the spin polarized calculations.[37] The MAE is determined by performing non-collinear total energy calculations including SOC with magnetic axes along

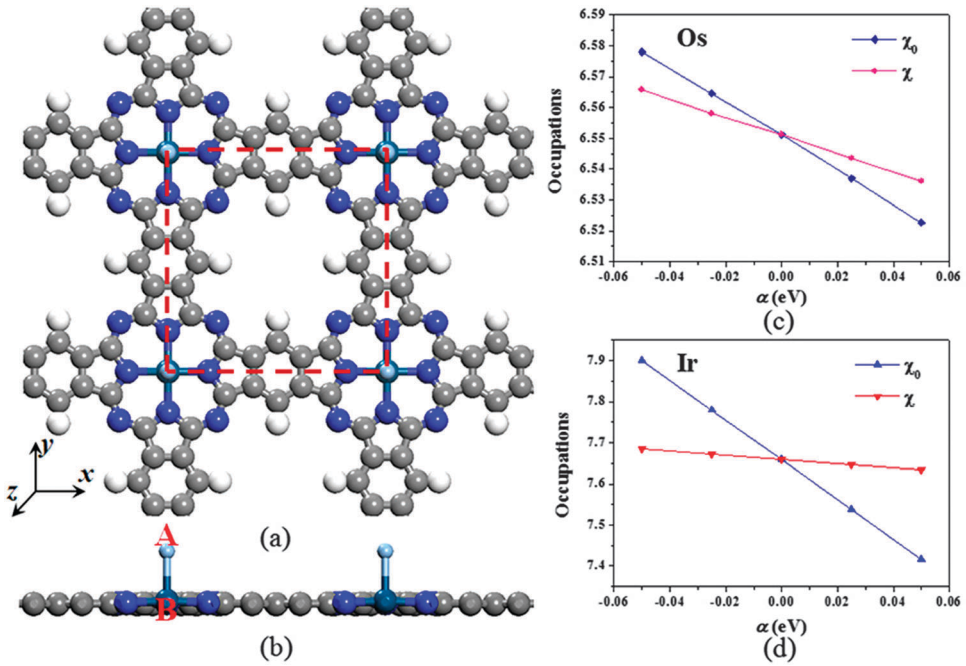

Fig. 1 (a) Top view and (b) side view of the poly-(A,B)Pc framework. Red dashed square represents the simulating unit cell. Occupations on A atom with respect to perturbation parameter α of (c) poly-(Os,B)Pc and (d) poly-(Ir,B)Pc.

x and z directions, denoted as $E_{\parallel}$ and $E_{\perp}$, respectively. The integration in the reciprocal space is conducted by summing over the Γ-centered Monkhorst–Pack k point meshes[38] with density less than $2\pi \times 0.01$ Å^{-1} along periodic x and y directions. Convergence was tested using different k point meshes to ensure accurate computed MAE values. We find that finer k point meshes yield MAE values varying within 0.1 meV, which corresponds to less than 1% error in most cases discussed in this work. We also note that this k point mesh density has been well verified in previous works.[25,26,39] The geometric structure is relaxed using the conjugated gradient method without any symmetry constraint until the Hellmann–Feynman force on each atom is smaller than 0.01 eV Å^{-1}. Our calculation procedure has been verified by comparing with previous results.[24,30]

The on-site Coulomb repulsion parameter, Hubbard U, is used to correct for strong correlation of the magnetic 5d orbital. The value of U is often semi-empirical and is generally obtained by comparing with experimental results. In addition, it varies with different bonding environments. Since no experimental results are available for the poly-TMPc systems, we determine Hubbard U self-consistently from first-principles using the linear response approach proposed by Cococcioni and Gironcoli.[40] Here the total on-site occupation is considered and the effective Hubbard U can be written as

$$U = \frac{\mathrm{d}^2 E\left[\{n^I\}\right]}{\mathrm{d}(n^I)^2} - \frac{\mathrm{d}^2 E_0\left[\{n^I\}\right]}{\mathrm{d}(n^I)^2}, \quad (1)$$

where n^I is the localized state occupation in the d orbital of site I. E and E_0 are the total energy functionals in the interacting and non-interacting Kohn–Sham equation, respectively,

$$E\left[\{n^I\}\right] = \min_{\alpha_I}\left\{E\left[\{n^I\}\right] - \sum_I \alpha_I n^I\right\}, \quad (2)$$

$$E_0\left[\{n^I\}\right] = \min_{\alpha_{I,0}}\left\{E_0\left[\{n^I\}\right] - \sum_I \alpha_{I,0} n^I\right\}. \quad (3)$$

α_I is the Lagrange multiplier with

$$\frac{\mathrm{d}E\left[\{n^I\}\right]}{\mathrm{d}n^I} = -\alpha_I, \quad \frac{\mathrm{d}^2 E\left[\{n^I\}\right]}{\mathrm{d}n^I} = -\frac{\mathrm{d}\alpha_I}{\mathrm{d}n^I}, \quad (4)$$

$$\frac{\mathrm{d}E_0\left[\{n^I\}\right]}{\mathrm{d}n^I} = -\alpha_{I,0}, \quad \frac{\mathrm{d}^2 E_0\left[\{n^I\}\right]}{\mathrm{d}n^I} = -\frac{\mathrm{d}\alpha_{I,0}}{\mathrm{d}n^I}. \quad (5)$$

Using α as a perturbation parameter, we introduce the (interacting and non-interacting) density response function of the system as,

$$\chi^I = \frac{\mathrm{d}n_I}{\mathrm{d}\alpha_I}, \quad \chi_0^I = \frac{\mathrm{d}n_I}{\mathrm{d}\alpha_{I,0}}. \quad (6)$$

The effective interaction parameter U of site I can then be rewritten as,

$$U = \frac{\mathrm{d}\alpha_{I,0}}{\mathrm{d}n_I} - \frac{\mathrm{d}\alpha_I}{\mathrm{d}n_I} = \left[\chi_0{}^{-1} - \chi^{-1}\right]^I. \quad (7)$$

We use this linear response approach to the total on-site occupation as implemented in the Quantum-ESPRESSO (QE) code[41] to self-consistently calculate the U value of the atom A in the poly-(A,B)Pc. The GGA-PBE exchange–correlation functional and PAW method are used. The wave-function and electron density cutoff energies are set as 60 Ry and 240 Ry, respectively. Test calculations show that adding a Hubbard U on the atom B change the MAE value only marginally. Therefore, we only apply the Hubbard U on the atom A.

III. Results

First we briefly discuss the preferred absorption site of a 5d TM atom on the poly-TMPc. Due to large d–d orbital interactions, the 5d TM atom binds strongly with the central embedded TM atom. On the contrary, since the Pc sheet is aromatic, the 5d TM atom binds weakly with the organic part. By taking the poly-(Ir,Rh)Pc as an example (Fig. S1 in the ESI†), we find that if the Ir atom is initially placed on top of a N atom, after relaxation it moves to on top of Rh. This configuration is furthermore found to be energetically lower than when the 5d TM resides on the hexagon and pyrrole pentagon by 0.26 and 0.91 eV, respectively. Hence, the structure shown in Fig. 1a and b illustrates the most stable poly-(A,B)Pc framework that can be realized experimentally. In Fig. 1c and d we plot the 5d orbital occupation with respect to the perturbation parameter α. We see that both the occupations in interacting and non-interacting systems are linear, and the density response function χ can be calculated from the inverse of their slope. In this way, using eqn (7) the effective U values for Os and Ir are calculated to be 1.6 eV and 2.5 eV, respectively. We also find that these values are almost insensitive to different atoms substituted at the B site.

Next we discuss the geometric and electronic structures of the poly-(A,B)Pc sheets. After relaxation, we find that in all systems the Pc framework remains flat, while the atom B is slightly lifted by the atom A (by less than 0.3 Å). The bond lengths between the N atom in the Pc sheet and the central TM atom B ($d_{\mathrm{N-B}}$), as well as that between the adsorbed A and the central atom B ($d_{\mathrm{A-B}}$) are listed in Table 1. Note that all the $d_{\mathrm{N-B}}$ values lie in the range between 1.9–2.1 Å, and no Jahn–Teller distortion is observed. As for the $d_{\mathrm{A-B}}$, all the relaxed bond lengths are in the range of 2.2–2.5 Å.

As discussed in our previous work,[19] the Pc framework tends to attract two electrons from the embedded TM atom in order to retain its aromaticity and flat geometry. We perform charge analysis by integrating electron density around the nuclei within its Wigner–Seitz cell. This analysis reveals that the total number of electrons transferred from both atoms A and B to the Pc framework lie in the range of 1.5–2.0 $|e|$ (Table 1), showing result consistent with that estimated from chemical aromaticity. In detail, we see that the atom A donates more than one electron, while the atom B provides less than one electron. Furthermore, when atom B belongs to the Fe-group, the q_{B} is smaller than that when B is in the Co-group. In this case the atom B carries around eight valence electrons. All the structures are magnetic. Magnetic moments of atom A and B (m_{A} and m_{B}) are listed in Table 1. We see that the atom A carries most of the magnetic moment in the unit cell, while the atom B and the Pc framework only carry small

Table 1 Relaxed bond lengths between N in Pc sheet and central atom B (d_{N-B}), between A and B (d_{A-B}), electron population on A and B (q_A and q_B), magnetic moment on atom A and B, and that in one unit cell (m_A, m_B, and m_{cell}), and calculated MAE of poly-(A,B)Pc

Atom A	Os						Ir					
Atom B	Fe	Co	Ru	Rh	Os	Ir	Fe	Co	Ru	Rh	Os	Ir
d_{N-B} (Å)	1.954	1.939	2.011	1.995	2.012	1.997	1.962	1.945	2.016	2.001	2.014	2.002
d_{A-B} (Å)	2.223	2.392	2.306	2.472	2.314	2.476	2.228	2.492	2.313	2.464	2.330	2.459
q_A ($\|e\|$)	1.3	1.2	1.3	1.2	1.2	1.2	1.1	1.1	1.1	1.1	1.1	1.0
q_B ($\|e\|$)	0.5	0.6	0.4	0.8	0.4	0.5	0.6	0.7	0.5	0.9	0.5	0.5
m_A (μ_B)	3.1	2.5	3.1	2.4	3.0	2.4	2.0	1.9	2.0	1.8	1.9	1.8
m_B (μ_B)	0.6	0.0	0.4	0.1	0.4	0.1	0.7	0.1	0.5	0.1	0.4	0.1
m_{cell} (μ_B)	4.0	3.0	4.0	3.0	4.0	3.0	3.0	2.0	3.0	2.0	3.0	2.0
MAE (meV)	−36.6	−29.3	1.8	−32.0	−5.7	−22.3	−11.5	2.6	−20.4	2.0	−31.3	−24.7

magnetic moment. When A = Os, its magnetic moment ($m_{A=Os}$) becomes ~3 μ_B since it is in +1 valence state and carries ~7 electrons. On the other hand, when A = Ir, similar analysis yields $m_{A=Ir}$ to be ~2 μ_B. For the atom B, our previous works[19,23] showed that the degeneracy of its five d orbitals can be lifted to "4+1" in the planar square crystal field, where only the $d_{x^2-y^2}$ orbital is higher in energy while the other four orbitals have relatively lower energies. In this case, when the atom B has around eight electrons, they fill the lower four orbitals and carry small magnetic moments. This also explains why different Hubbard U values on the atom B yield almost the same result as those of the systems stated previously. We find that the atom A and B couple ferromagnetically. Contributions of atom A, atom B, and the Pc framework yield total magnetic moment in one unit cell to be 4.0 (3.0) μ_B when A = Os and B in the Fe–(Co–) group, and to be 3.0 (2.0) μ_B when A = Ir and B is in the Fe–(Co–) group (Table 1). In Fig. 2 we plot spin density of poly-(Os,Os)Pc and poly-(Ir,Ir)Pc sheets, where we see that spin densities are mainly localized on TM-d orbitals.

Next we performed magnetic non-collinear calculations with SOC to find the MAE and the easy axis of magnetization. Since use of different Hubbard U values can lead to quite different MAE values (see Fig. S2 in the ESI†), we focus on the results obtained by using self-consistently determined U value. We find that in most cases the MAE value is negative, indicating that the magnetic easy axis lies parallel to the x–y plane (Table 1). Only three of the systems studied possess small positive MAE values with the largest value being 2.6 meV in the poly-(Ir,Co)Pc.

In order to increase the MAE values of the systems, we explore two strategies; applying an external vertical electric-field or a bi-axial tensile strain. First, we discuss the effect of electric (E) field pointing from the 5d TM to the Pc plane (inset of Fig. 3b).

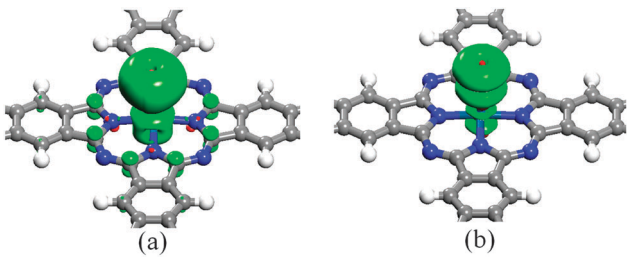

Fig. 2 Spin density of (a) poly-(Os,Os)Pc and (b) poly-(Ir,Ir)Pc in isosurface (value of 0.02 |e| Å^{-3}) form, with green and red representing spin up and spin down channels, respectively.

Taking poly-(Ir,Rh)Pc as an example, we find that most magnetic moments still localize around the Ir atom. In addition, E-field redistributes the electrons in the system. In Fig. 3a we plot the electron redistribution density $\Delta\rho$ ($=\rho_{E\text{-field}=1.0} - \rho_{E\text{-field}=0}$), where we observe that the electrons underneath the Ir atom (Ir–Rh bond) move up to the Ir atom, and the electrons under the poly-RhPc plane move up to the plane. Note that the order of magnitude of electric field applied in our study (a few volts per nm) is comparable with the experimentally achieved range.[42,43] Taking poly-(Ir,Rh)Pc as an example, we carefully checked that if E-field may cause any structural instability. We perturbed the structure in various ways, applied an E-field of 1.0 V Å^{-1}, and then optimized the system. After full relaxation, we did not find any structural instability of poly-(Ir,Rh)Pc and the Pc framework still remained planar. The resulting MAE values of the poly-(Ir,Ir)Pc, poly-(Ir,Rh)Pc, and poly-(Os,Os)Pc are significantly enhanced (Fig. 3b). For example, for the MAE of poly-(Ir,Ir)Pc sheet, when the E-field increases from 0.0 to 0.4 V Å^{-1}, is enhanced from −24.7 meV to 0.0 meV; further increasing the E-field up to 1.0 V Å^{-1} greatly enhances the MAE to 122.2 meV. Similarly, with an applied E-field of 1.0 V Å^{-1}, the MAE of poly-(Ir,Rh)Pc and poly-(Os,Os)Pc can be enhanced to 143.4 and 34.4 meV, respectively. We plot the relative energy difference with respect to magnetic axis azimuth angle θ of the three systems in Fig. 3c. For each system, as the magnetic axis direction goes from vertical to parallel to the plane, the total energy increases monotonically. This shows that below the blocking temperature the magnetic axis can be locked along the z and $-z$ directions. These two states can work as "0" and "1" states in magnetic storage devices. In addition, since the unit cell lattice constant is large (>10 Å), the coupling between nearest neighbor Ir (or Os) is small. As a result, the magnetic axis can be tuned individually by using a magnetic tip.

We now consider the second strategy to enhance MAE by applying biaxial tensile strain (Fig. 4a). Unlike previous results in poly-TMPc systems,[22] we observe no spin crossover on the 5d TM atoms in this system under tensile strain. To check if any structural instability takes place under a 10% tensile strain, we considered poly-(Ir,Rh)Pc as an example. We used a (2 × 2 × 1) supercell and perturbed the structure in various ways and then optimized its geometry. The Pc framework remained flat without buckling, confirming the stability of our systems under tensile strain. We find that biaxial strain can enhance the MAE of both the poly-(Ir,Ir)Pc and poly-(Ir,Rh)Pc systems. For the poly-(Ir,Ir)Pc, the MAE is increased from −24.7 meV in its strain-free state to

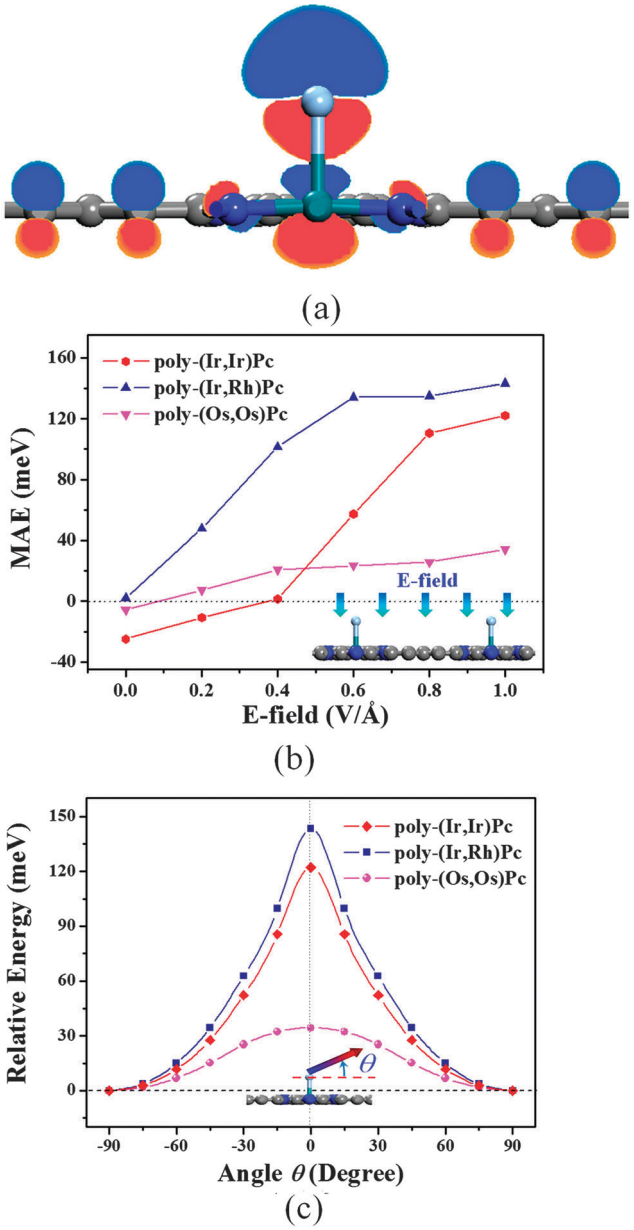

Fig. 3 (a) A slice of the E-field induced electron redistribution density $\Delta\rho$ in poly-(Ir,Rh)Pc, where blue (red) represents $\Delta\rho$ value larger (smaller) than 0.01 (−0.01) |e| Å^{-3}. (b) Variation of MAE with respect to the magnitude of the E-field of poly-(Ir,Ir)Pc, poly-(Ir,Rh)Pc, and poly-(Os,Os)Pc. (c) Relative energy change for the magnetic axis pointing along different directions. Inset shows the azimuth angle θ of the magnetic axis.

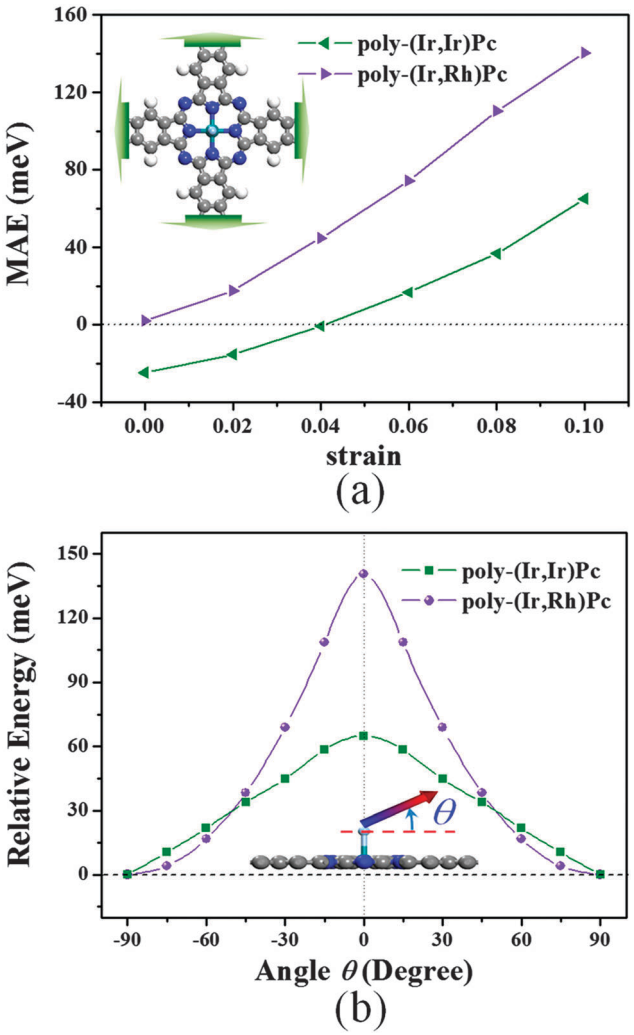

Fig. 4 (a) Dependence of MAE on biaxial tensile strain of poly-(Ir,Ir)Pc and poly-(Ir,Rh)Pc. (b) Relative energy change with respect to magnetic axis pointing along different directions. Inset shows the azimuth angle θ of the magnetic axis.

approximately zero under biaxial strain of 4%. Larger strain can further make its MAE to be positive, and the MAE becomes 65.0 meV under biaxial strain of 10%. As for the poly-(Ir,Rh)Pc system, we find that the biaxial tensile strain can also increase its MAE. When 3% strain is applied, its MAE value is enhanced to 25 meV. The MAE can be increased further to 140.5 meV under a 10% biaxial tensile strain. We also plot the relative energy difference with respect to magnetic axis azimuth angle θ in Fig. 4b. Note that the total energy decreases monotonically when the azimuth angle of the magnetic axis increases from 0° to 90°.

It is also known that 3d TM-based clusters are good candidates for magnetic storage and memory devices.[44,45] One may wonder that instead of Ir or Os, if a 3d TM adsorbed on the poly-TMPc sheet can also lead to large MAE values. By using similar approach, we calculated the MAE values of poly-(Fe,Fe)Pc and poly-(Co,Co)Pc frameworks to be −3.2 and 0.0 meV, respectively. We also calculated their variation under E-field and under tensile strain. Unfortunately, we observed only marginal changes of the MAE values. Hence, we propose that the large SOC of 5d TM is a key factor to achieve giant MAE.

We now discuss the origin of this giant MAE. The MAE value can be regarded as the difference between vertical and in-plane interactions of the spin–orbit coupling[46]

$$\mathrm{MAE} = \xi^2 \sum_{\mathrm{u,o};\alpha,\beta} (2\delta_{\alpha\beta} - 1) \left[\frac{|\langle \mathrm{u},\alpha|\hat{L}_z|\mathrm{o},\beta\rangle|^2 - |\langle \mathrm{u},\alpha|\hat{L}_x|\mathrm{o},\beta\rangle|^2}{\varepsilon_{\mathrm{u},\alpha} - \varepsilon_{\mathrm{o},\beta}} \right], \quad (8)$$

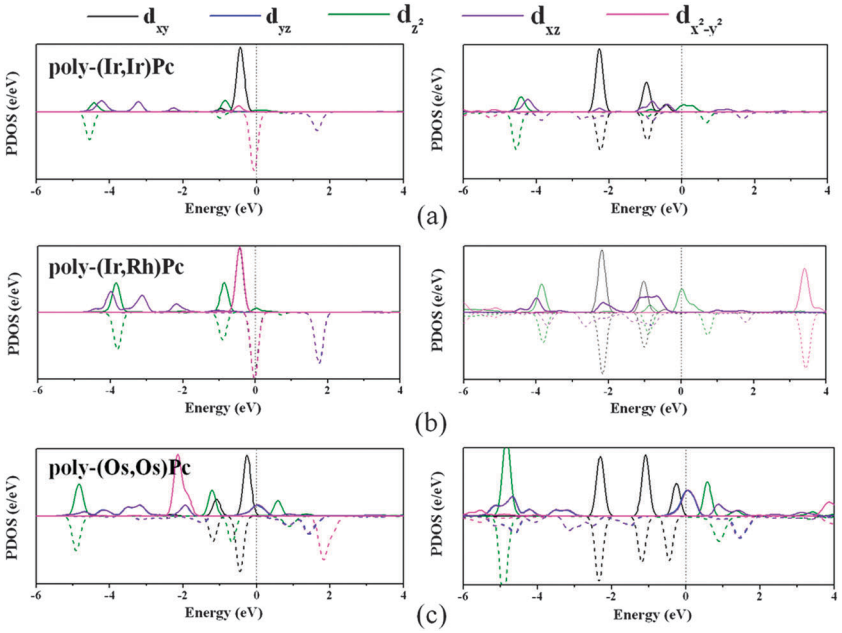

Fig. 5 Projected density of states of atom A (left panel) and atom B (right panel) in (a) poly-(Ir,Ir)Pc, (b) poly-(Ir,Rh)Pc, and (c) poly-(Os,Os)Pc under E-field of 1.0 V Å^{-1}.

where $\varepsilon_{u,\alpha}$ ($\varepsilon_{o,\beta}$) is the energy level of the unoccupied (occupied) spin α (spin β) state, and ξ is the magnitude of spin–orbit coupling. As much of the magnetism originates from d orbitals, we calculated different d orbital contributions to MAE. By using spherical harmonics, Y_l^m, d orbitals can be written as

$$\begin{aligned} d_{xy} &= \left[Y_2^{-2} + Y_2^2\right]/\sqrt{2}, \quad d_{x^2-y^2} = i\left[Y_2^{-2} - Y_2^2\right]/\sqrt{2}, \\ d_{xz} &= \left[Y_2^{-1} - Y_2^1\right]/\sqrt{2}, \quad d_{yz} = i\left[Y_2^{-1} + Y_2^1\right]/\sqrt{2}, \\ d_{z^2} &= Y_2^0. \end{aligned} \tag{9}$$

By calculating the orbital interaction term $\left|\langle d_1|\hat{L}_z|d_2\rangle\right|^2 - \left|\langle d_1|\hat{L}_x|d_2\rangle\right|^2$, we find that if the d_1 and d_2 orbitals are in the same spin channel, the interactions between d_{xy} and $d_{x^2-y^2}$, and that between d_{xz} and d_{yz} give positive contribution to MAE. On the other hand, if d_1 and d_2 are in different spin channels, interactions between d_{xy} and d_{yz}, between $d_{x^2-y^2}$ and d_{yz}, and between d_{yz} and d_{z^2} can increase the MAE value. From the denominator of eqn (8), it can be seen that the most dominant contribution to the MAE comes from the orbitals around the Fermi level. Hence, in Fig. 5 we plot the projected density of states (PDOS) of TM atoms in poly-(Ir,Ir)Pc, poly-(Ir,Rh)Pc, and poly(Os,Os)Pc under E-field of 1.0 V Å^{-1}. We see that due to structural symmetry, the two d_π (d_{xz} and d_{yz}) bands as well as the d_{xy} and $d_{x^2-y^2}$ bands of atom A are degenerate. We clearly observe that the giant positive MAEs in both poly-(Ir,Ir)Pc and poly-(Ir,Rh)Pc systems are mainly due to the interaction between d_{xy} and $d_{x^2-y^2}$ orbitals of the absorbed Ir (atom A) in the spin down channel, while in the poly-(Os,Os)Pc the large positive

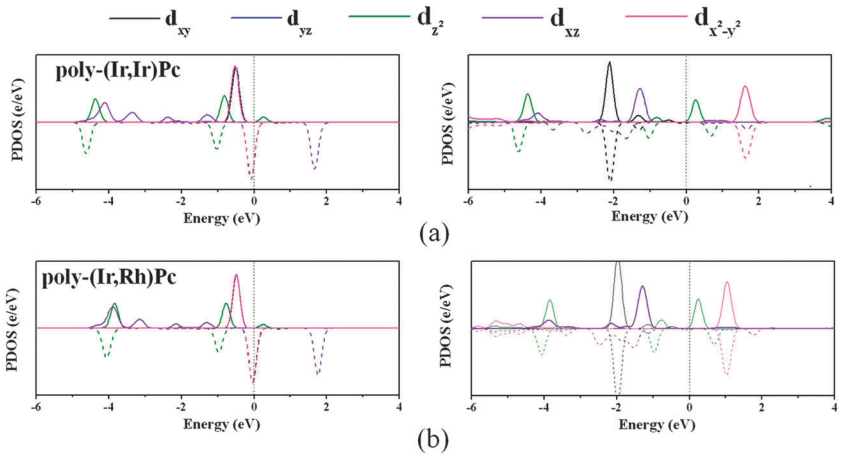

Fig. 6 PDOS of atom A (left panel) and atom B (right panel) in (a) poly-(Ir,Ir)Pc and (b) poly-(Ir,Rh)Pc under biaxial tensile strain of 10%.

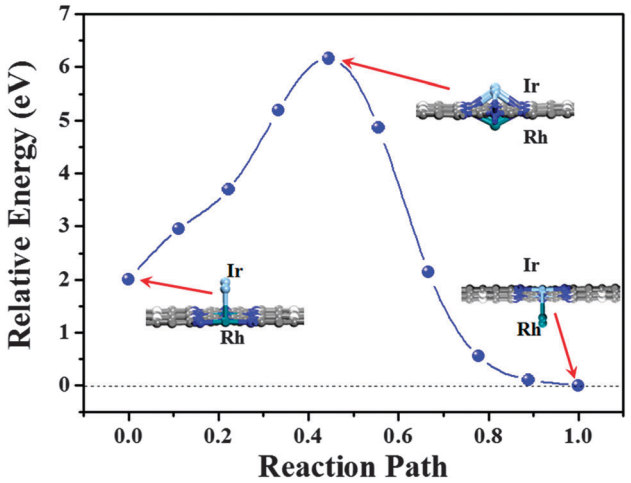

Fig. 7 Energy profile for reversing the sites of Ir and Rh – from poly-(Ir,Rh)Pc to poly-(Rh,Ir)Pc.

MAE originates from the interaction between spin up d_{xz} and d_{yz} of the absorbed Os (atom A). As for the strain induced MAE, similar coupling between the spin down d_{xy} and $d_{x^2-y^2}$ of the absorbed Ir (atom A) leads to the giant MAE values in poly-(Ir,Ir)Pc and poly-(Ir,Rh)Pc (Fig. 6). We also see that the in-plane atom B contributes slightly to the MAE value.

We now briefly discuss the stability of the systems. Since the Pc framework is aromatic and π conjugated, it is unlikely that the atom A would move away from the atom B. However, it is still possible that the atom A and B can switch their positions to form poly-(B,A)Pc. Taking poly-(Ir,Rh)Pc as an example, we calculated the energy profile for such a transition using nudged elastic band method (Fig. 7).[47] We find that although the total energy of poly-(Ir,Rh)Pc is higher than poly-(Rh,Ir)Pc by about 2 eV in one unit cell, the energy barrier is calculated to be 4.16 eV, showing the metastability of the poly-(Ir,Rh)Pc. This high energy barrier is due to the strong binding between the Pc sheet and the Rh atom. Hence, we conclude that the other poly-(A,B)Pc systems are stable.

IV. Conclusion

In summary, using first-principles density functional theory, we have systematically calculated the magnetocrystalline anisotropy energy (MAE) of 5d transition metal (TM) atoms (Os and Ir) adsorbed on polymerized TM-based phthalocyanine framework. For the strongly correlated magnetic TM atoms, we have incorporated Hubbard *U* term using a self-consistent linear response approach. We find that all the systems possess either negative or small positive MAE which hinders their practical application in magnetic memory and storage devices. We then explored two strategies to enhance the MAE value. These strategies are (i) applying intermediate vertical external electric field or (ii) biaxial tensile strain. The former yields MAE values of 122.2 meV, 143.4 meV, and 34.4 meV for poly-(Ir,Ir)Pc, poly-(Ir,Rh)Pc, and poly-(Os,Os)Pc, respectively. The latter, on the other hand, yields MAE values of 65.0 meV and 140.5 meV for poly-(Ir,Ir)Pc and poly-(Ir,Rh)Pc systems, respectively. The giant MAEs are attributed to the interactions between the spin down d_{xy} and $d_{x^2-y^2}$ orbitals in poly-(Ir,Ir)Pc and poly-(Ir,Rh)Pc, and between the spin up d_{xz} and d_{yz} orbitals in poly-(Os,Os)Pc. The stability of these systems has been verified by calculating the energy barrier for switching the Ir and Rh atom sites in poly-(Ir,Rh)Pc. We emphasize that the benefit of using these phthalocyanine based polymers is that the TM atoms occupy well defined sites in the Pc sheet which prevents them from clustering. In contrast to previous theoretical studies where metal atoms occupy regular vacancy sites in graphene or BN which are difficult to achieve experimentally, the systems we have studied can be fabricated experimentally. We hope that the present work will stimulate experimental interest and we look forward to validation of our theoretical prediction.

Acknowledgements

This work is partially supported by grants from the U.S. Department of Energy, Office of Basic Energy Sciences, Division of Materials Sciences and Engineering under Award # DE-FG02-96ER45579, grants from the National Natural Science Foundation of China (NSFC-11174014, NSFC-21273012), and the National Grand Fundamental Research 973 Program of China (2012CB921404). The authors thank the crew of the Center for Computational Materials Science, the Institute for Materials Research, Tohoku University (Japan), for their continuous support of the HITACHSR11000 supercomputing facility.

References

1 J. V. Barth, G. Costantini and K. Kern, *Nature*, 2005, **437**, 671–679.
2 W.-G. Wang, M. Li, S. Hageman and C. L. Chien, *Nat. Mater.*, 2012, **11**, 64–68.
3 I. G. Rau, S. Baumann, S. Rusponi, F. Donati, S. Stepanow, L. Gragnaniello, J. Dreiser, C. Piamonteze, F. Nolting, S. Gangopadhyay, O. R. Albertini, R. M. Macfarlane, C. P. Lutz, B. A. Jones, P. Gambardella, A. J. Heinrich and H. Brune, *Science*, 2014, **344**, 988–992.
4 J. W. Colson, A. R. Woll, A. Mukherjee, M. P. Levendorf, E. L. Spitler, V. B. Shields, M. G. Spencer, J. Park and W. R. Dichtel, *Science*, 2011, **332**, 228–231.
5 E. L. Spitler and W. R. Dichtel, *Nat. Chem.*, 2010, **2**, 672–677.
6 S. S.-Y. Chui, S. M.-F. Lo, J. P. H. Charmant, A. G. Orpen and I. D. Williams, *Science*, 1999, **283**, 1148–1150.
7 L. Grill, M. Dyer, L. Lafferentz, M. Persson, M. V. Peters and S. Hecht, *Nat. Nanotechnol.*, 2007, **2**, 687–691.
8 T. Kambe, R. Sakamoto, K. Hoshiko, K. Takada, M. Miyachi, J.-H. Ryu, S. Sasaki, J. Kim, K. Nakazato, M. Takata and H. Nishihara, *J. Am. Chem. Soc.*, 2013, **135**, 2462–2465.
9 Z. F. Wang, Z. Liu and F. Liu, *Nat. Commun.*, 2013, **4**, 1471–1475.
10 K. Sato, L. Bergqvist, J. Kudrnovsky, P. H. Dederichs, O. Eriksson, I. Turek, B. Sanyal, G. Bouzerar, H. Katayama-Yoshida, V. A. Dinh, T. Fukushima, H. Kizaki and R. Zeller, *Rev. Mod. Phys.*, 2010, **82**, 1633–1690.

11 B. K. Rao and P. Jena, *Phys. Rev. Lett.*, 2002, **89**, 185504.
12 A. V. Krasheninnikov, P. O. Lehtinen, A. S. Foster, P. Pyykko and R. M. Nieminen, *Phys. Rev. Lett.*, 2009, **102**, 126807.
13 J. He, N. Jiao, C. Zhang, H. Xiao, X. Chen and L. Sun, *J. Phys. Chem. C*, 2014, **118**, 8899–8906.
14 Y. Wang and Y. Ding, *Ann. Phys.*, 2014, **526**, 415–422.
15 D. Hao, C. Song, Y. Ning, Y. Wang, L. Wang, X.-C. Ma, X. Chen and Q.-K. Xue, *J. Chem. Phys.*, 2011, **134**, 154703.
16 Y.-L. Wang, J. Ren, C.-L. Song, Y.-P. Jiang, L.-L. Wang, K. He, X. Chen, J.-F. Jia, S. Meng, E. Kaxiras, Q.-K. Xue and X.-C. Ma, *Phys. Rev. B: Condens. Matter Mater. Phys.*, 2010, **82**, 245420.
17 M. Abel, S. Clair, O. Ourdjini, M. Mossoyan and L. Porte, *J. Am. Chem. Soc.*, 2011, **133**, 1203–1205.
18 M. Koudia and M. Abel, *Chem. Commun.*, 2014, **50**, 8565–8567.
19 J. Zhou and Q. Sun, *J. Am. Chem. Soc.*, 2011, **133**, 15113–15119.
20 K. Lü, J. Zhou, L. Zhou, Q. Wang, Q. Sun and P. Jena, *Appl. Phys. Lett.*, 2011, **99**, 163104.
21 Y. Li and Q. Sun, *Sci. Rep.*, 2014, **4**, 4098.
22 J. Zhou, Q. Wang, Q. Sun, Y. Kawazoe and P. Jena, *J. Phys. Chem. Lett.*, 2012, **3**, 3109–3114.
23 J. Zhou and Q. Sun, *Nanoscale*, 2014, **6**, 328–333.
24 P. Błoński and J. Hafner, *Phys. Rev. B: Condens. Matter Mater. Phys.*, 2009, **79**, 224418.
25 R. Xiao, M. D. Kuzmin, K. Koepernik and M. Richter, *Appl. Phys. Lett.*, 2010, **97**, 232501.
26 R. Xiao, D. Fritsch, M. D. Kuzmin, K. Koepernik, H. Eschrig and M. Richter, *Phys. Rev. Lett.*, 2009, **103**, 187201.
27 I. Beljakov, V. Meded, F. Symalla, K. Fink, S. Shallcross, M. Ruben and W. Wenzel, *Nano Lett.*, 2014, **14**, 3364–3368.
28 T. O. Strandberg, C. M. Canali and A. H. Macdonald, *Nat. Mater.*, 2007, **6**, 648–651.
29 Y. Zhang, Z. Wang and J. Cao, *J. Mater. Chem. C*, 2014, **2**, 8817–8821.
30 J. Hu and R. Wu, *Nano Lett.*, 2014, **14**, 1853–1858.
31 J. Hu and R. Wu, *Phys. Rev. Lett.*, 2013, **110**, 097202.
32 S. L. Dudarev, G. A. Botton, S. Y. Savrasov, C. J. Humphreys and A. P. Sutton, *Phys. Rev. B: Condens. Matter Mater. Phys.*, 1998, **57**, 1505–1509.
33 J. P. Perdew, K. Burke and M. Ernzerhof, *Phys. Rev. Lett.*, 1996, **77**, 3865–3868.
34 G. Kresse and J. Furthmuller, *Phys. Rev. B: Condens. Matter Mater. Phys.*, 1996, **54**, 11169–11186.
35 P. E. Blöchl, *Phys. Rev. B: Condens. Matter Mater. Phys.*, 1994, **50**, 17953–17979.
36 G. Kresse and D. Joubert, *Phys. Rev. B: Condens. Matter Mater. Phys.*, 1999, **59**, 1758–1775.
37 S. H. Vosko, L. Wilk and M. Nusair, *Can. J. Phys.*, 1980, **58**, 1200–1211.
38 H. J. Monkhorst and J. D. Pack, *Phys. Rev. B: Solid State*, 1976, **13**, 5188–5192.
39 P. Ruiz-Diaz, T. R. Dasa and V. S. Stepanyuk, *Phys. Rev. Lett.*, 2013, **110**, 267203.
40 M. Cococcioni and S. de Gironcoli, *Phys. Rev. B: Condens. Matter Mater. Phys.*, 2005, **71**, 035105.
41 P. Giannozzi, S. Baroni, N. Bonini, M. Calandra, R. Car, C. Cavazzoni, D. Ceresoli, G. L. Chiarotti, M. Cococcioni, I. Dabo, A. Dal Corso, S. de Gironcoli, S. Fabris, G. Fratesi, R. Gebauer, U. Gerstmann, C. Gougoussis, A. Kokalj, M. Lazzeri, L. Martin-Samos, N. Marzari, F. Mauri, R. Mazzarello, S. Paolini, A. Pasquarello, L. Paulatto, C. Sbraccia, S. Scandolo, G. Sclauzero, A. P. Seitsonen, A. Smogunov, P. Umari and R. M. Wentzcovitch, *J. Phys.: Condens. Matter*, 2009, **21**, 395502.
42 F. Xia, D. B. Farmer, Y.-m. Lin and P. Avouris, *Nano Lett.*, 2010, **10**, 715–718.
43 Y. Zhang, T.-T. Tang, C. Girit, Z. Hao, M. C. Martin, A. Zettl, M. F. Crommie, Y. Ron Shen and F. Wang, *Nature*, 2009, **459**, 820–823.
44 J. M. Zadrozny, D. J. Xiao, M. Atanasov, G. J. Long, F. Grandjean, F. Neese and J. R. Long, *Nat. Chem.*, 2013, **5**, 577–581.
45 M. Atanasov, D. Aravena, E. Suturina, E. Bill, D. Maganas and F. Neese, *Coord. Chem. Rev.*, 2015, **289–290**, 177–214.
46 D. S. Wang, R. Wu and A. J. Freeman, *Phys. Rev. B: Condens. Matter Mater. Phys.*, 1993, **47**, 14932–14947.
47 G. Mills, H. Jonsson and G. K. Schenter, *Surf. Sci.*, 1995, **324**, 305–337.